

# Structural Relationships of Actin, Myosin, and Tropomyosin Revealed by Cryo-Electron Microscopy

R. A. Milligan and P. F. Flicker

Department of Cell Biology, Sherman Fairchild Building, Stanford University School of Medicine, Stanford, California 94305

**Abstract.** We have calculated three-dimensional maps from images of myosin subfragment-1 (S1)-decorated thin filaments and S1-decorated actin filaments preserved in frozen solution. By averaging many data sets we obtained highly reproducible maps that can be interpreted simply to provide a model for the native structure of decorated filaments. From our results we have made the following conclusions. The bulk of the actin monomer is  $\sim 65 \times 40 \times 40$  Å and is composed of two domains. In the filaments the monomers are strongly connected along the genetic helix with weaker connections following the long pitch helix. The long axis of the monomer lies roughly perpendicular to the filament axis. The myosin head (S1) approaches the actin filament tangentially and binds to a single

actin, the major interaction being with the outermost domain of actin. In the map the longest chord of S1 is  $\sim 130$  Å. The region of S1 closest to actin is of high density, whereas the part furthest away is poorly defined and may be disordered. By comparing maps from decorated thin filaments with those from decorated actin, we demonstrate that tropomyosin is bound to the inner domain of actin just in front of the myosin binding site at a radius of  $\sim 40$  Å. A small change in the azimuthal position of tropomyosin, as has been suggested by others to occur during  $\text{Ca}^{2+}$ -mediated regulation in vertebrate striated muscle, appears to be insufficient to eclipse totally the major site of interaction between actin and myosin.

**I**N muscle, the asynchronous cyclic interaction of myosin crossbridges with the thin (actin-containing) filaments is responsible for contraction. Calcium regulates the interaction of the molecules in vertebrate striated muscle by acting on the troponin-tropomyosin complex in the thin filament. Contraction is fueled by ATP hydrolysis and is thought to involve a conformational change (a power stroke) of the myosin head while it is bound to the actin filament. Direct evidence for the proposed structural changes is lacking and studies have concentrated on the interaction of the molecules in rigor. This tightly bound state, formed in the absence of ATP, is believed to be the conformation at the end of the power stroke and thus represents a single well-defined state in the crossbridge cycle.

In vitro, myosin subfragment-1 (S1)<sup>1</sup> binds to F-actin and thin filaments (actin, tropomyosin, and troponin) assuming a rigor-like conformation and exhibiting an arrowhead appearance in the electron microscope. Using the helical symmetry of the filaments, several groups of workers have calculated three-dimensional (3-D) maps by computer processing images of negatively stained specimens (Amos et al., 1982;

Moore et al., 1970; Taylor and Amos, 1981; Toyoshima and Wakabayashi, 1985a, b; Vibert and Craig, 1982). From these investigations two general models describing the interaction of the proteins have emerged. In one model (Huxley, 1972), S1 approaches the actin filament tangentially and binds to a single actin monomer. Tropomyosin is attached to actin in front of the S1 binding site. In the second model (Amos et al., 1982), the geometry of binding is "end-on" rather than tangential. A single S1 binds to two actin monomers. Tropomyosin is thought to lie within the curve formed by the S1 head, i.e., behind the actin-S1 binding site. Maps presented by other groups show some features of both models (Taylor and Amos, 1981; Toyoshima and Wakabayashi, 1985a, b; Vibert and Craig, 1982; see Amos, 1985 for review). The reason for the lack of agreement about the structure is not clear but may be due to variability of preservation in negative stain coupled with, in some instances, insufficient data averaging.

We present here a study of the native structure of S1-decorated thin filaments and S1-decorated actin filaments. We have examined filaments frozen in thin aqueous films in the electron microscope at low temperature. By averaging data from many images, we have obtained maps of the native density distribution in which the structural details are highly reproducible. These maps can be interpreted simply, allowing us to describe some of the features of the actin and S1 molecules and the geometry of their interaction in decorated fila-

Dr. Milligan's present address is Department of Molecular Biology, Research Institute of Scripps Clinic, 10666 N. Torrey Pines Rd., La Jolla, CA 92037.

1. *Abbreviations used in this paper:* CTF, contrast transfer function; 3-D, three-dimensional; LL, layer-line; MRDD, mean radial density distribution; S1, myosin subfragment-1.

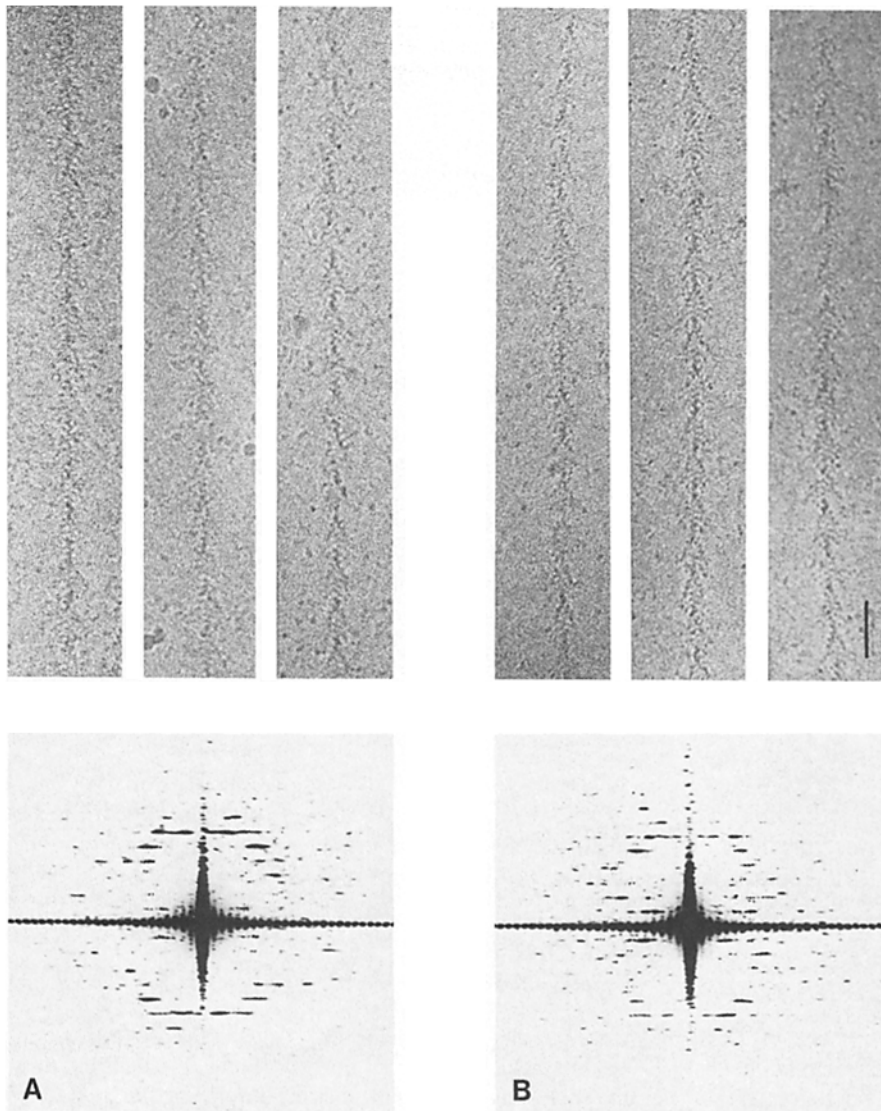


Figure 1. Images and representative optical diffraction patterns of (A) S1-decorated thin filaments and (B) S1-decorated actin filaments. Bar, 500 Å.

ments. In addition, we have determined the position of tropomyosin by comparing the maps from decorated thin filaments with those from decorated actin. We discuss our findings in relation to current views of thin filament-based regulation of contraction.

## Materials and Methods

### Proteins

We prepared native thin filaments from glycerinated rabbit myofibrils following, with some modifications, the procedure described by Kendrick-Jones et al. (1970). Glycerol was removed by washing the myofibrils in a large volume of solution containing 10 mM imidazole pH 7.0, 50 mM KCl, 1 mM MgCl<sub>2</sub>, 0.5 mM EGTA, 1 mM dithiothreitol. After a short, low-speed centrifugation the myofibrils were resuspended in the same buffer, containing in addition 5 mM Mg-ATP, 0.1 mM phenylmethylsulfonyl fluoride, and 0.1 μg/ml pepstatin. The suspension was homogenized on ice with a Sorvall Omnimixer at maximum speed for a total of 20 s. The homogenate was centrifuged for 10 min at 7,000 g followed by 50 min at 30,000 g to pellet thick filaments. The supernatant, containing mostly thin filaments, was stored on ice.

Electrophoretically pure actin was provided by J. A. Spudich and co-

workers (Stanford University). It had been prepared from rabbit muscle acetone powder by the method of Spudich and Watt (1971). Before use the F-actin was recycled following the procedure described by Pardee and Spudich (1982). F-actin was used as a 0.1–0.2 mg/ml solution in 10 mM imidazole pH 7.4, 100 mM KCl, 1 mM MgCl<sub>2</sub>, 50 μM CaCl<sub>2</sub>, 0.2 mM Na-ATP, 0.5 mM β-mercaptoethanol.

S1 was a gift from D. A. Winkelmann (University of Medicine and Dentistry of New Jersey). It had been prepared from chicken muscle as described by Winkelmann et al. (1983) and was supplied as a lyophilized powder. SDS PAGE confirmed that the samples contained the S1 heavy chain and a full complement of light chains. For use, the S1 was dissolved at a concentration of 10 mg/ml in 10 mM imidazole pH 7.0, 50 mM KCl, 1 mM MgCl<sub>2</sub>, 1 mM CaCl<sub>2</sub>, 0.5 mM dithiothreitol (S1 buffer), and dialyzed overnight against the same buffer. The solution was centrifuged at 12,000 g for 10 min to remove aggregates and diluted to a final concentration of 0.5–0.6 mg/ml in the same buffer immediately before use.

### Specimen Preparation and Electron Microscopy

Thin filaments or F-actin at a concentration of 0.1–0.2 mg/ml were adsorbed for 0.5–2 min to carbon-coated holey films that had previously been glow discharged in an atmosphere of amyl-amine (Lepault et al., 1983). Each grid was rinsed gently with 10 drops of S1 buffer to dilute out ATP, then two to three drops of S1 solution (0.5–0.6 mg/ml) were applied. After ~2 min the grids were blotted and quick-frozen in liquid ethane slush (Lepault

Table I. Summary of Parameters Obtained during Image Processing and Averaging

Filament	No. of helical repeats	Tilt‡	Phase residual§	$\Delta\phi$	$\Delta z$ ¶	Radial scale factor	Amplitude scale factor**	Phase residual§	Radial scale factor	Amplitude scale factor**
		Degrees	Degrees	Degrees	Å			Degrees		
Decorated thin filaments, series A										
16331	5	0	18	-2	-1	0.97	0.84	20	1.03	1.01
16332	5	1.5	20	-5	-0.5	1.00	1.00	15	1.03	1.25
16371	8	0	29	-2	-1	0.99	1.06	13	1.01	0.93
16372	6	0.9	25	-8	-2	1.01	0.93	18	0.99	1.15
16461	6	1.2	16	-0.5	0	1.00	1.00	15	1.02	1.24
16463*	5	-1	20	-9	-2	1.01	0.97	11	0.99	1.35
16611	10	-0.6	24	2	0	0.98	1.10	16	0.99	0.97
16781	8	2	20	5	-1	1.04	0.89	14	0.98	1.28
Decorated thin filaments, series B										
9112	7	-1.2	15	0	2	0.99	0.94	19	0.99	1.45
15432	4	-0.35	19	4.5	0.5	0.98	1.03	20	1.05	1.80
86972	6	1.5	20	0.5	-3	0.99	1.02	12	1.00	1.22
86973	10	-2.5	24	6	1	0.99	0.99	16	1.04	0.91
87332	7	3	24	-1	-3	1.00	1.12	16	0.98	1.13
87333	7	0.5	29	-1	-2	0.98	0.97	13	0.99	1.23
87971*	7	0	20	5.5	3	0.99	1.02	17	0.98	1.13
91785	9	-1	23	-8.5	4	1.04	0.92	18	1.00	1.05
Decorated actin										
51233	6	0	22	-2	-4	0.95	0.92	17	1.03	1.92
53771	6	3.5	20	-1	-1	0.98	1.12	18	1.09	1.02
56722	6	-1	26	-1	2	1.06	1.09	13	1.03	1.22
57231	5	1.3	17	3	0	0.99	1.08	20	1.00	1.46
61381*	6	2	23	5	-2	1.01	1.21	19	1.00	0.96
61382	7	1	16	4	1	1.06	0.97	15	1.01	0.89
61383	5	0.3	17	-3	2	0.99	1.11	17	1.03	1.03
61384	10	-2.1	23	3	0	0.97	1.33	16	1.05	0.86

In the table headings, the fourth through the eighth parameters were obtained by comparing the near and far sides of individual filaments. The last three parameters were obtained by comparing near-far-side averages with the preliminary series average.

\* The filament in each series, which was used as the reference for calculation of the preliminary average.

‡ The tilt of the filament axis out of the object plane.

§ Amplitude-weighted mean phase residual (the parameter  $Q$  defined by DeRosier and Moore, 1970).

|| The rotation required for best fit of the two data sets being compared.

¶ The translation required for best fit of the two data sets being compared.

\*\* Within each series this scale factor was calculated using data from LLs 1, 2, 4, 5, 6, and 7. NB, When scaling the decorated actin data with the decorated thin filament data, LLs 4, 5, 6, and 7 only were used.

et al., 1983; Milligan et al., 1984). Carrying out these operations in a cold room at 4°C, as well as rapid transfer of the grid into the cryogen with a guillotine-like device, ensured minimal concentration of solutes by evaporation. Grids prepared in this way were stored under liquid nitrogen until required.

Grids were mounted under liquid nitrogen in either a Philips cold holder (PW 6500/00) or a Gatan cryo-transfer system (model 626; Gatan, Inc., Warrendale, PA) and examined in a Philips EM 400 equipped with an additional, twin-blade, anticontamination device (Homo et al., 1984) and operating at 100 kV. A 50- $\mu$ m objective aperture was used. Using strict low-dose conditions, images of thin vitreous ice spanning holes were recorded on Kodak SO163 film. Nominal magnifications were 33,000–45,000. The actual magnifications were determined from images of tobacco mosaic virus in frozen solution. The images were recorded 1.6–2.2  $\mu$ m underfocus. Care was taken to photograph small holes so that the level of defocus could be determined later by comparing the diffraction pattern from the carbon adjacent to the hole with a reference focal series. Film was developed in undiluted D19 developer for 10–12 min. Each area photographed received a total dose of <10 e/Å<sup>2</sup>.

### Image Processing

Three series of micrographs—two series of decorated thin filaments and one series of decorated actin filaments—were computer processed independently. As the processing followed the same overall scheme for each series of images, the operations carried out on a single series will be outlined in the following paragraphs.

Optimally defocused images showing minimal drift and astigmatism were examined directly and by optical diffraction, and suitable filaments were chosen for computer processing. Such filaments (Fig. 1) were fully decorated, i.e., showed a characteristic arrowhead appearance, and had straight regions 4–10 repeats long that gave diffraction patterns that were reasonably symmetric about the meridian and showed at least the seventh layer-line (1/51 Å). Areas of images containing the filaments were converted to optical density arrays with a microdensitometer (Perkin-Elmer Corp., Instrument Div., Norwalk, CT) using spot and step sizes of 25  $\mu$ m. The arrays were displayed and the filaments boxed and floated (using the average optical density of the perimeter of the box) into large arrays (512  $\times$  256) suitable for subsequent Fourier transformation. Care was taken during boxing to include only an integral number of helical repeats and to use a box that was wide enough (equivalent to  $\sim$ 400 Å) to include details of the structure that might not be clearly visible on the image.

We processed a large number of filaments. For each filament we measured the helical repeat and the ratio of the meridional intercepts of layer-line (LL) 6 and LL 1. The mean values of these parameters for the decorated thin filaments were 371.78 Å ( $\pm$ 7.203) and 6.307 ( $\pm$ 0.108), respectively, and for decorated actin filaments, 367.6 Å ( $\pm$ 6.757) and 6.231 ( $\pm$ 0.113), respectively. The small differences between the two specimens are significant at the 5% level. The values for the LL 6/LL 1 ratios that we obtained are similar to published values obtained from negatively stained filaments and confirm that the filaments do not conform exactly to either 13/6 or 28/13 helical geometry. However, to simplify processing and following the example of other workers, we processed the filaments assuming 13/6 helical geometry. For the helical repeat we used 370 Å.

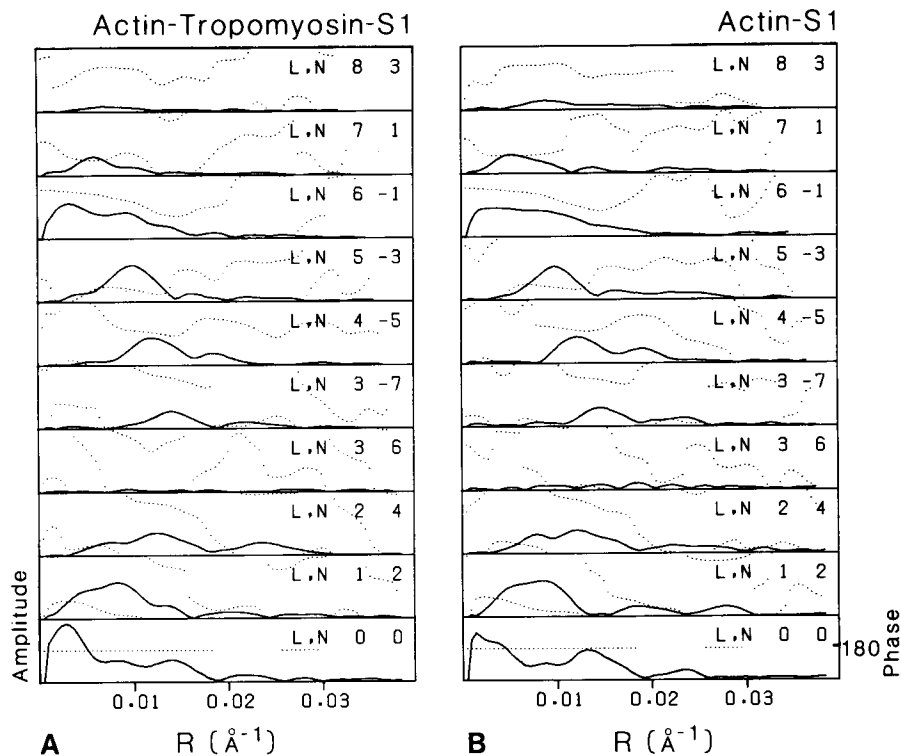


**Figure 2.** Amplitudes (solid curves) and phases (dotted curves) obtained by averaging 32 data sets (16 filaments) from decorated thin filaments (A) and 16 data sets (eight filaments) from decorated actin filaments (B). L is the layer-line number and N is the Bessel order indexed according to 13/6 helical geometry. The data along each layer-line have been truncated at a radial spacing of  $0.038 \text{ \AA}^{-1}$ , which is close to the first zero of the contrast transfer function. The peak positions and relative peak heights on the layer lines compare well with x-ray data from SI-labeled insect flight muscle (Amos et al., 1982; Goody et al., 1985). In particular, amplitude profiles along LLs 4, 5, 6, and 7 are very similar to the x-ray data. LL 1 profiles from electron microscopy data are of lower amplitude. Although this may be explained partly by CTF effects, some differences are expected, as  $\sim 50\%$  of diffracting SI moieties in the x-ray experiment were from endogenous myosin and appear to have more highly ordered tails than the exogenous SI.

Helical processing was carried out in the standard way (see e.g., DeRosier and Moore, 1970; Taylor and Amos, 1981; Vibert and Craig, 1982) using a suite of programs written originally at MRC, Cambridge. Briefly, layer-lines were extracted from computed transforms, the phase origin was centered on the helical axis, and corrections made to account for tilt of the filament out of the object plane. These latter corrections were  $<3.5^\circ$  (Table I). From each filament processed two data sets were obtained: one from the near side and one from the far side. By comparing the relative positions of the phase origins and the agreement between the phases of the near and far side data, a procedure known as "fitting," the degree of preservation of each filament can be assessed. Well-preserved filaments required only small relative movements of the origin of the far side data set, corresponding in real space to  $<10^\circ$  of rotation about the helical axis ( $\Delta\phi$ ) and  $<5 \text{ \AA}$  of translation along the axis ( $\Delta z$ ), to align it with the near side data (Table I). At such positions the amplitude-weighted mean phase residual, calculated from data over the strong peaks on LLs 1, 2, 4, 5, 6, and 7, was  $<30^\circ$  (Table I) and differed from the residual at the position expected for perfect preservation ( $\Delta\phi = 0^\circ$ ,  $\Delta z = 0 \text{ \AA}$ ) by only a few degrees. During averaging of the near and far sides, the contributions from the sixth and seventh Bessel orders, which both lie on LL 3, were separated (Amos and Klug, 1974).

### Averaging Data

The near-far-side averages were compared and the following criteria used to select a group to average together. The peak amplitudes of the data sets were normalized and the relative peak amplitude and peak position on each layer-line noted. The near-far-side average whose peak amplitudes and peak positions matched most closely the mean values for each layer-line was chosen as the reference data set. Data sets whose values were at the extremes of the distributions of amplitudes and positions were discarded. The remaining data sets were scaled together, aligned with the reference set, and corrections made to account for small differences in magnification of the images before averaging them. This preliminary average was then used as the reference and all data sets realigned and scaled to it. The parameters obtained from this procedure (Table I) were used to align and scale the data sets before the final round of averaging. In the fitting procedure the search for optimal correspondence of the data sets was carried out within relative rotations and translations equivalent to, at most, two turns of the short pitch helix. Because of this restricted search, data on the layer-lines originating from features with a similar repeat to the crossover distance, i.e., the tropomyosin complex in the decorated thin filament, were lost. The final decorated

thin filament and decorated actin maps were calculated from layer-line data obtained by averaging 16 and 8 near-far-side averages, respectively (Fig. 2). All layer-lines were included at full weight. In the maps we assigned the molecular boundary to the contour level which enclosed the total volume the proteins should occupy (assuming  $0.81 \text{ D/\AA}^3$  [Vibert and Craig, 1982]).

### Testing the Programs

To test the reliability of the programs, we calculated a side projection of the final map and wrote a grey-level image of this on to film. We thus created the equivalent of an electron micrograph of the final map. This "micrograph" was then processed in exactly the same manner as the real images had been and the resultant map compared with the map from which it was derived. The two maps were identical, demonstrating that the data were not degraded during the processing and that the programs appear to be error-free.

### Reliability of the Equatorial Data

The layer-line through the origin of the transform (the equator) consists, to the resolution of this study, of the zero order Bessel function and defines the mean radial density distribution (MRDD) of the structure. The major effects of these data in the 3-D maps are to alter the relative strengths of features at different radii and to change slightly the radial positions of some peaks. The data affect neither the azimuthal nor axial positions of features in the map. With negatively stained specimens there are indications that the equatorial data are unreliable. The presence of "forbidden" reflections in the diffraction pattern is believed to be a result of flattening or other anisotropic distortions of the specimen (Toyoshima and Wakabayashi, 1985a; Vibert and Craig, 1982); such deviations from cylindrical symmetry seriously affect the equatorial data. These observations, together with other uncertainties about the precise way in which stain surrounds the specimen (Trus and Steven, 1984), have resulted in a lack of agreement on how the equatorial data from stained specimens should be treated. Some workers have excluded these data and substituted model data (Taylor and Amos, 1981), whereas others have included them at half weight (Toyoshima and Wakabayashi, 1985a; Vibert and Craig, 1982).

Cryo-electron microscopy of unstained material appears to circumvent the flattening and selective staining problems associated with negative staining. Maps from images of acetylcholine receptors (Brisson and Unwin, 1985), gap junctions (Unwin and Ennis, 1984), and ribosomes (Milligan, 1985) in frozen solution show that the dimensions perpendicular to the car-

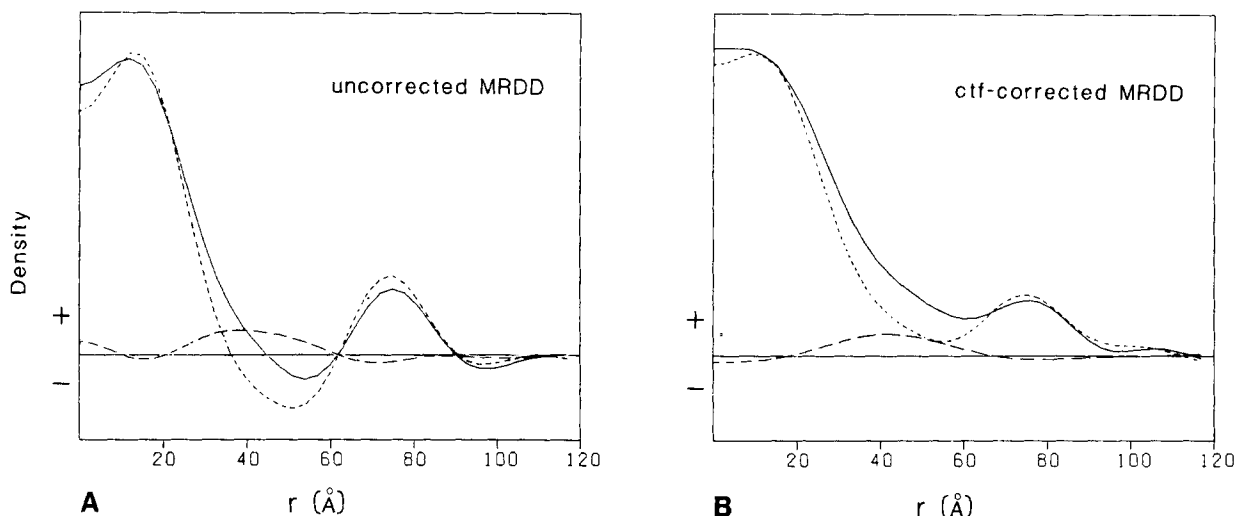


**Figure 3.** Plots of the MRDDs of the decorated filaments calculated from the equatorial data (A) before and (B) after the amplitudes have been adjusted to compensate for the effects of the contrast transfer function (see Materials and Methods). The results from decorated thin filaments (solid curves), decorated actin filaments (dotted curves), and the difference data (dashed curves) are shown. The MRDD calculated from the difference data peaks at a radius of  $\sim 40$  Å.

bon film are close to those measured by x-ray diffraction from specimens in solution. In this study we have made the following additional observations. During blotting, a concave lens of liquid is formed over the holes in the support film. We have observed that with dilute suspensions, the specimen tends to equilibrate in the thicker part of the lens, i.e., in an area of the aqueous film where the interaction of the specimen with the surface of the liquid is minimized. In other words, given free movement, particles or filaments in the film tend to “avoid” areas where they would be flattened. We also note that the data-set averages consistently lack significant “forbidden” reflections on the meridian (compare Fig. 2 with equivalent figure in Vibert and Craig, 1982), suggesting that the filaments are not distorted. We therefore conclude that images of helical specimens in frozen solution can provide reliable equatorial data.

### Effects of the Contrast Transfer Function (CTF)

Since the micrographs were recorded  $\sim 1.9$   $\mu\text{m}$  underfocus, the transforms calculated from the images are modulated by the effects of the CTF. To the resolution of this study only the calculated amplitudes are affected, and primarily those closest to the origin of the transform. These data can be corrected provided that the relative contributions to the image from phase contrast, amplitude contrast, and aperture contrast are known. Although the precise values are not known for frozen specimens, we estimate that phase effects contribute  $\sim 85$ – $90\%$  of the contrast. To explore the effects of such an estimate on the maps, we adjusted the layer-line data accordingly (Erickson and Klug, 1971), computed maps, and compared these with maps calculated from uncorrected data. As a result of the correction, the negative peaks in the map, which are a consequence of underfocussing, were attenuated. This effect is evident when the MRDDs from maps with and without the CTF correction are compared (Fig. 3). The other major effect of the correction was a change in the relative strengths of features radially. The molecular boundary in the corrected maps (the contour enclosing the predicted volume of the proteins) excludes weak high radius features which are present in all the maps we have calculated (Fig. 4) and which are significantly above background density. The exclusion of these reproducible features from the molecular boundary reduces the length of SI in the maps to  $\sim 110$  Å,  $\sim 60$ – $65\%$  of the expected length (Elliot and Offer, 1978; Flicker et al., 1983). Clearly the CTF correction gives a result that is incompatible with the dimensions of the SI molecule. One possible explanation for this observation is that the filaments possess disorder which increases with filament radius. Such a phenomenon might account for the under-emphasis of the high radius features in the corrected maps. Most importantly, the CTF correction we explored resulted in only small changes in the azimuthal, axial, and radial positions of density peaks in the maps and therefore did not alter our assignments for either the actin monomer or SI (see Fig. 6, B and C).

We emphasize that our conclusions about the structural relationships of the proteins in decorated filaments are the same whether or not we correct for the effects of the CTF. Because of uncertainties about the precise relative contributions of amplitude, aperture, and phase contrast to the image and about the effects of disorder, we have chosen to present the uncorrected data and maps derived from it.

### Investigation of Differences

To show the position of tropomyosin, a difference data set was obtained by subtracting the decorated actin layer line data (Fig. 2 B) from the decorated thin filament data (Fig. 2 A) and a 3-D map calculated from it. Alignment and scaling of the data sets were carried out using LLs 4, 5, 6, and 7 only. In each section of the difference map there were two positive peaks whose peak densities were about twice the absolute value of the highest negative peak.

In a more analytical approach we investigated the differences between the two structures using statistical methods. All near-far-side averages were scaled together and brought to the same phase origin. 3-D maps of the two structures, consisting of the mean and standard deviation of the density at 10-Å intervals in  $x$ ,  $y$ , and  $z$  and occupying at least one helical repeat, were calculated. Using the Student's  $t$  test, densities at equivalent points in the two maps were compared and a 3-D array of  $t$  generated. This “ $t$  map” was contoured and interpreted with reference to a Student's  $t$  table. As a control, the  $t$  test was used to compare the two series of decorated thin filament data.

Calculation of a difference map and the statistical analysis were also carried out after the amplitudes along all the layer-lines had been adjusted, as described earlier, to compensate for the effects of the CTF (data not shown). Results equivalent to those presented here were obtained.

### Results

Images of SI-decorated filaments in frozen solution (Fig. 1) show a characteristic arrowhead appearance. The contrast in the images is low; consequently, the optical diffraction patterns (Fig. 1) and the layer-line data obtained by processing single filaments (not shown) are noisy. 3-D maps calculated from individual data sets or from near-far-side averages show many nonreproducible features. To reduce this noise to a low level we found it necessary to average a number of data sets. We determined the number of data sets required to accomplish this by comparing two independent maps of the deco-

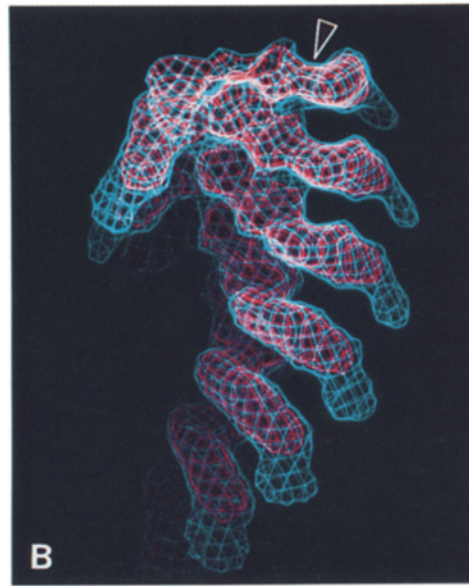
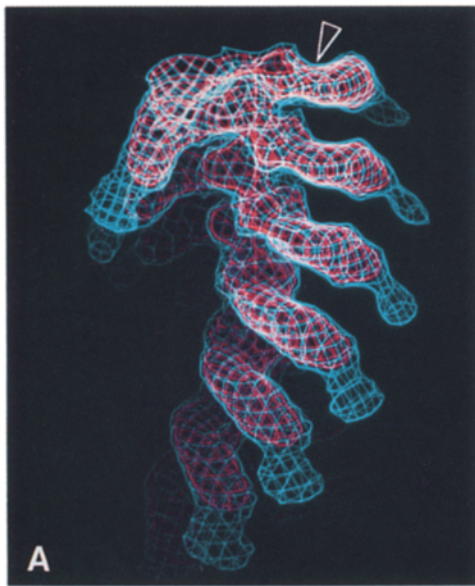


**Figure 4.** Oblique views of about one repeat of the 3-D map of (A) the decorated thin filament and (B) the decorated actin filament. The top of each map is tilted towards the observer by  $\sim 35^\circ$ . The boundary contour (blue) encloses the total volume the proteins should occupy. The inner contour (red) is at a level corresponding to 15% of the peak density within the boundary. Note that this contour does not extend into the region of S1 lying at high radius. The longest chord of S1 is  $\sim 130 \text{ \AA}$  and makes an angle of  $\sim 42^\circ$  with the filament axis. When data are adjusted to compensate for the effects of the CTF, the low density, high radius domain is not included within the boundary. Regions of the map at a lower radius than the constriction (arrows) represent the thin filament and F-actin.

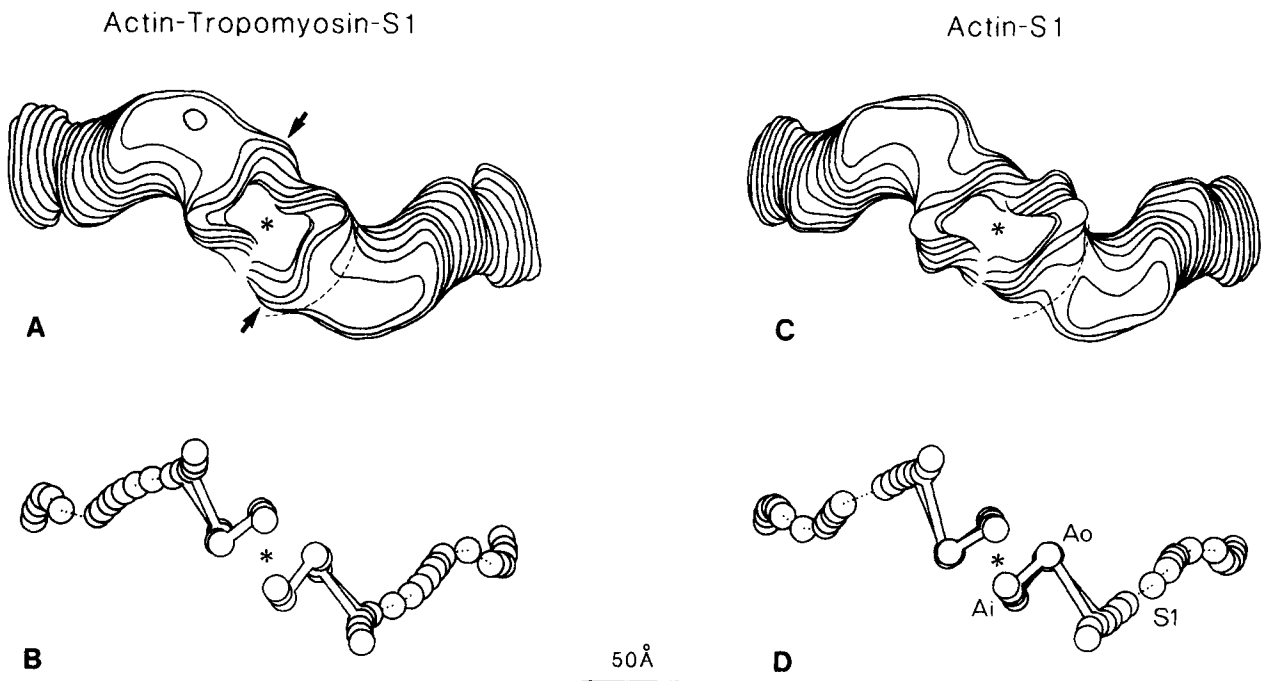


**Figure 5.** Views of the 3-D maps of (A) decorated thin filaments and (C) decorated actin as the structure would appear looking towards the Z line in muscle fibers. The molecular surfaces shown are the same as those contoured in blue in Fig. 4. In each drawing are two successive repeating units along the genetic helix of the decorated filament, i.e., two actin molecules and two S1 molecules. The boundary between actin and myosin is estimated to be located at a radius of  $\sim 45 \text{ \AA}$  (dotted arcs). In the decorated thin filament map there is extra density lying in front of the binding site (arrows in A). B and D are plots of the locations of the density peak(s) in each 5-Å-thick section through the structure. This representation shows the locations of the inner (Ai) and outer (Ao) domains of actin, the tangential approach of the S1 to the actin filament, and the major linkages between the parts of the structure. It should be noted that adjustments to the data aimed at compensating for the effects of the CTF affect the molecular boundaries shown in A and C; low radius features are emphasized and high radius features are attenuated. In contrast, the peak positions and the connectivities between the parts of the structure are relatively insensitive to such adjustments. The plots in B and D are therefore accurate representations of the molecular "skeletons."

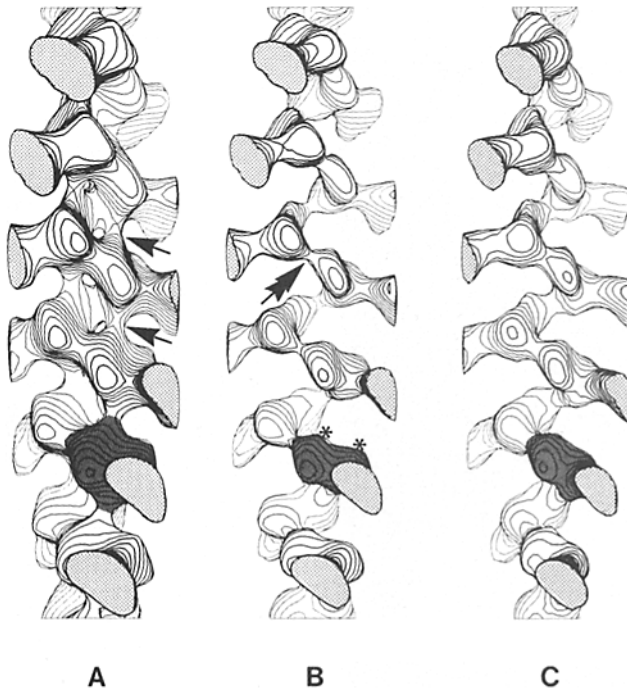


**Figure 6.** Orientation and connectivity between actin monomers. One crossover ( $370 \text{ \AA}$ ) of the central part of the decorated actin map is shown to a radius of  $54 \text{ \AA}$ . If the entire S1 were present the resultant arrowhead motif would point upwards. The 3-D distribution of high densities was displayed with hidden lines removed. Maps *A* and *B* are at density levels corresponding to  $\sim 20$  and  $\sim 40\%$ , respectively, of the highest density within the molecular boundary (derived from calculations on the entire decorated actin map). Areas associated with a single actin monomer are darkly stippled. The lightly stippled areas following the long pitch helix represent the cut ends of the S1 stumps. Weak long pitch connections between actin monomers (*single arrows*) are not seen in map *B*. Stronger connections following the genetic helix (*double arrow*) are evident in both *A* and *B*. Asterisks on map *B* identify the two density domains that we conclude, on the basis of their intimate association, represent a single actin monomer. Map *C* was calculated from data adjusted to compensate for the effects of the CTF and is displayed at a level comparable to that in *B*. Although there are minor differences, the assignment of the actin monomer and the relative strengths of the contacts between monomers are unchanged. The decorated thin filament data gave equivalent results.

rated thin filament. Each author separately prepared specimens, imaged them, processed the images, and averaged data to provide the two maps for the comparison. The maps were virtually identical when each was obtained by averaging between 12 and 16 data sets (six to eight filaments). The amplitude-weighted mean phase residual when the two 16-data-set averages were compared was  $9^\circ$ , attesting to the great similarity of the averages. Maps obtained by averaging fewer data sets showed differences due to noise, making an interpretation of the density details impossible. Averaging a larger number of data sets than 16 did not alter the result. We therefore concluded that 12–16 data sets (from six to eight well-preserved filaments) were sufficient to calculate a highly reliable map of the reproducible details of these decorated filaments. Accordingly, the layer-line data used to calculate a map of the decorated actin filaments (Fig. 2 *B*) are the average of 16 data sets (eight filaments). Layer-line data for the

decorated thin filament map (Fig. 2 *A*) are the average of all 32 data sets (16 filaments) used in the preliminary work.

The eighth layer-line ( $0.0216 \text{ \AA}^{-1}$ ) is present in both of the final data set averages giving an axial resolution of  $\sim 46 \text{ \AA}$  in the maps. Radially the data extend to  $0.038 \text{ \AA}^{-1}$ . Although the amplitudes at the extremes of the layer-lines are low, the phases show reasonably good agreement, suggesting that  $26\text{--}30 \text{ \AA}$  is a realistic estimate of the resolution in this direction. The data presented here have not been adjusted to compensate for the effects of image defocus as the relative amounts of amplitude, aperture, and phase contrast contributing to the image at low spatial frequencies is in doubt. However, we did explore the effects of an estimated correction and found that, whereas the boundary of the structure changed somewhat, the positions of density peaks and the relative strengths of connections between them were minimally affected (see Materials and Methods). In view of this result, we have concentrated our attention on the structural relationships of the proteins comprising the decorated filaments. In the following sections we compare the decorated actin map with the decorated thin filament map and describe their similarities and differences.

### Common Features of the Maps

The 3-D maps (Figs. 4 and 5) of decorated thin filaments and of decorated actin filaments are almost identical in most of their structural features. Measured from the maps, the overall width of the decorated filaments is  $\sim 260 \text{ \AA}$ . Although plots of the MRDDs suggest that the diameter is somewhat less than this ( $\sim 220 \text{ \AA}$ ), the apparent discrepancy can be explained when the portion of S1 at high radius is examined. This portion is of very low density (Fig. 4) and, given its radial position, would be expected to make a very low contribution to the MRDD.

In the maps from both specimens we can distinguish a constriction at a radius of  $\sim 45 \text{ \AA}$  (Fig. 5, *A* and *C*). The simplest interpretation of this feature is that it represents the boundary between actin and S1. Plots of the density peaks in each section of the maps (Fig. 5, *B* and *D*) support this explanation since the positions of the peaks within and outside this radius and the major linkages between them preclude other interpretations.

Within the radius of the constriction lies the actin filament or the thin filament. In this region we distinguish two peaks of density in each repeating unit (Fig. 5, *B* and *D*). Since both peaks occur in both maps, they are clearly features of the actin monomer; tropomyosin is not resolved as a distinct peak in the decorated thin filament map. Calculating the distances of the peaks of one actin monomer from those in adjacent monomers and from the peak in S1 at the binding site allows us to estimate dimensions of  $65 \times 40 \times 40 \text{ \AA}$  for the bulk of the actin monomer. The presence of the two peaks suggests a two domain structure. To indicate the positions of the domains relative to the filament axis we refer to them as *A<sub>i</sub>* (inner) and *A<sub>o</sub>* (outer). The long axis of the monomer lies roughly perpendicular to the filament axis. There is weak connectivity between actin monomers along the long pitch helix and stronger linkages along the genetic helix (Fig. 6).

At higher radius than the constriction lies the elongated and slightly curved S1 molecule. We estimate the length of S1 in the maps to be  $\sim 130 \text{ \AA}$  (see Discussion). Internal density variations divide S1 into two domains or regions. At high

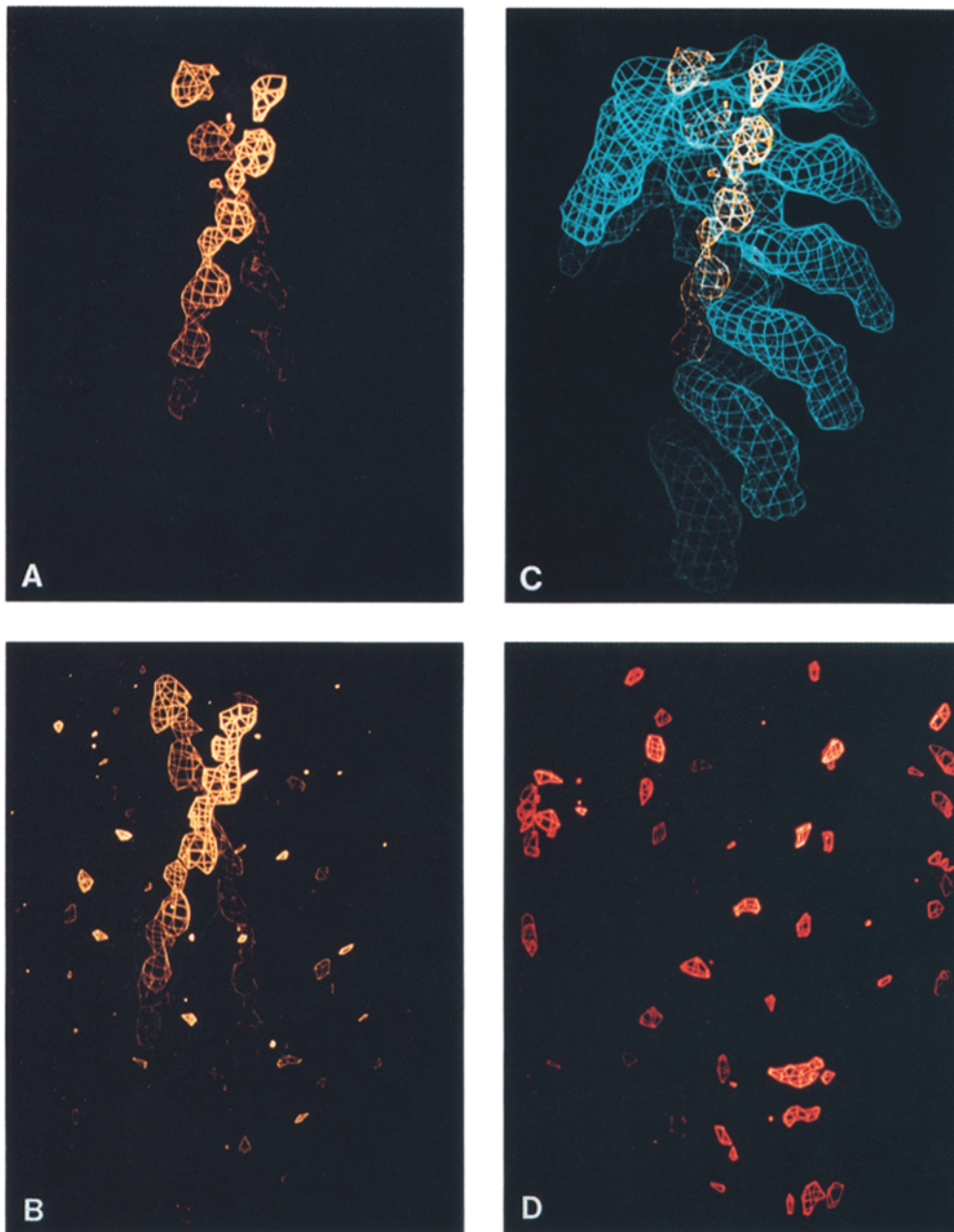


**Figure 7.** Differences between decorated thin filaments and decorated actin filaments. (A) 3-D map obtained by Fourier-Bessel inversion of the difference layer-line data. All layer-lines have been included at full weight. The map is contoured at a positive density level close to the absolute value of the highest negative peak. The contours enclose regions where there is additional material in decorated thin filaments. (B) “*t*” map obtained by comparing real-space averages of 16 decorated thin filaments and eight decorated actin filaments using the Student’s *t* test (see Materials and Methods). The yellow contour encloses regions where the probability that the differences between the two specimens are due to chance is  $<0.5\%$ . (C) The difference map (i.e., A) superimposed on the map of the decorated actin filament. (D) Results from a control experiment in which the eight maps comprising decorated thin filament series A were compared with the eight maps from decorated thin filament series B. The red contour is at the 1% significance level.

radius in the map, there is a region of very low density that is  $\sim 35\text{-}\text{\AA}$  long (measured in the same direction as the length of S1),  $\sim 25\text{-}\text{\AA}$  wide, and is extended or smeared azimuthally. The second domain of S1 is of high density. It can be described best as a slightly curved rod,  $\sim 95\text{-}\text{\AA}$  long and  $45\text{-}55\text{\AA}$  in diameter. This portion of S1 approaches the actin filament tangentially and attaches to a long face of a single actin monomer. The major contact is with the outer domain (Ao) of actin. When viewed down the filament axis (Fig. 5), the long axis of the actin monomer lies approximately parallel to the projection of the S1 portion of the structure. This view emphasizes the tangential nature of the interaction and the location of the attachment site on the long face of actin.

### Differences

Compositionally, the two specimens we have examined differ in that only the decorated thin filaments contain the tropo-

myosin-troponin regulatory complex. However, as the layer-line averaging procedure was carried out in a manner that resulted in the loss of data contributions from troponin (see Materials and Methods), we expect that any differences we find in the maps will be due to the presence of tropomyosin alone.

The layer-line data (Fig. 2) from which the two maps are calculated show small differences. These differences are located principally on the equator and on the first three layer-lines. The region on LL 2 between  $0.02$  and  $0.03\text{ \AA}^{-1}$ , where intensity changes in the x-ray diffraction pattern have been observed during activation of skeletal muscle (e.g., Kress et al., 1986; Vibert et al., 1972), shows higher amplitude in the data from tropomyosin-containing filaments. Other notable differences occur on LL 1 at  $0.013$  and  $0.028\text{ \AA}^{-1}$  and on the equator at  $0.003$ ,  $0.012$ , and  $0.024\text{ \AA}^{-1}$ . We used two approaches to investigate the features in the 3-D map to which

these differences relate. First, in a simple approach, we subtracted the decorated actin data from the decorated thin filament data to obtain difference data. The MRDD calculated from the equatorial difference data (Fig. 3, *dashed curve*) shows a major positive peak at a radius of  $\sim 40$  Å. The 3-D map calculated from the difference data (Fig. 7A) shows two strings of positive peaks following the long pitch helix. Although the result seemed clear, we felt that this simple approach might be misleading as it does not take into account the variability of individual data sets included in the two final averages.

To investigate this uncertainty we took a second, more analytical, approach. We made a statistical analysis of the near-far-side maps comprising the final averages and determined the location of differences based on probability levels (see Materials and Methods). As a control, and to determine the baseline noise level, we compared the two eight-filament averages of the thin filament data. From this control experiment the 3-D map of differences at the 1% significance level is shown in Fig. 7D. The small regions at this level are not in close proximity to the biological structure and seem to bear little relation to it. We have concluded that they are due to residual noise in the layer-line data or due to the limited sizes of the populations analyzed. In contrast, comparing the decorated thin filament maps with the decorated actin maps gives a clear result (Fig. 7B). The contours in Fig. 7B enclose regions where the probability that the differences are real and not due to chance is  $>99.5\%$ . These regions follow the long pitch helix and coincide with the positive peaks in the difference map. Thus both approaches point to the same location for the regulatory protein tropomyosin.

By superimposing the difference map on the map of decorated actin at the same phase origin (Fig. 7C), we conclude that in the decorated filaments studied here tropomyosin lies in front of the actin-myosin binding site at a radius of  $\sim 40$  Å. The molecule follows the path of the long pitch helix. At each repeating actin-S1 unit, tropomyosin makes contact with the Ai domain of the actin monomer.

## Discussion

We have studied the native structure of S1-decorated thin filaments and S1-decorated actin filaments by electron microscopy and image processing and present a model detailing the interaction of actin, S1, and tropomyosin in the rigor state. We have improved on previous work in several important ways. First, by freezing the filaments in thin aqueous films and examining them at low temperature, we obtained images of the filaments in their native state. We processed many images and averaged a large number of data sets to obtain the final maps of the structures. By comparing independently determined maps we found that 12–16 data sets were the minimum required to reduce contributions from noise to a low level in the final average map. Finally, we took two approaches to determine the position of tropomyosin in the decorated thin filament map: we calculated a map from the difference between the two final data set averages and we made a real-space, statistically based comparison of the individual maps making up each final average to determine the location of significant differences. These improvements in technique and experimental approach give maps of the native structure that are highly reproducible and can be interpreted

simply. In contrast, studies of negatively stained filaments have yielded results that have not always been in agreement (Amos et al., 1982; Moore et al., 1970; Taylor and Amos, 1981; Toyoshima and Wakabayashi, 1985a, b; Vibert and Craig, 1982).

We feel that the improvements we have made in methodology, coupled with the high reproducibility of our results, allow us to make a number of solid conclusions about the arrangement of actin and S1, together with the regulatory protein tropomyosin, in decorated filaments. Our maps also provide a framework that should assist in fitting together the high resolution crystal structures of actin and S1 which will be completed in the near future (Kabsch et al., 1985; Rayment and Winkelmann, 1984; Sakabe et al., 1983; Schutt et al., 1985).

## Actin

In our maps, the distribution of density peaks within and outside the constriction at a radius of  $\sim 45$  Å, coupled with information on the width of the actin filament from other sources (e.g., Trinick et al., 1986), dictate the assignment of the peaks as either actin or myosin (Fig. 5). Within a 45-Å radius the density associated with the most strongly connected peaks must represent the actin monomer. We are thus able to distinguish a single actin monomer and describe some of its features. The dimensions we estimate for the bulk of the monomer,  $\sim 65 \times 40 \times 40$  Å, are in accord with those from the x-ray crystal structure analysis of actin-DNase 1 co-crystals (Kabsch et al., 1985; Sakabe et al., 1983; Suck et al., 1981). As in the x-ray analysis we find that the monomer consists of two domains (Fig. 6). At the resolution of our maps we were unable to distinguish the larger domain, consisting of 60% of the total mass (Kabsch et al., 1985), from the smaller domain. The long axis of the actin monomer lies roughly perpendicular to the filament axis, a finding that confirms the results of a recent analysis of two frozen hydrated actin filaments by Trinick et al. (1986) and some but not all of the conclusions based on maps from negatively stained material (reviewed by Egelman, 1985). To date none of the maps are able to provide a unique solution of how to orient the currently available x-ray structure in the actin filament. It is, however, worth noting that the orientation of the monomers in the filaments described here is similar to the packing of actin molecules along a two-fold screw axis in co-crystals of actin and DNase 1 (Suck et al., 1981).

## Myosin Subfragment 1

The S1 we used in our experiments is a well-characterized molecule containing a full complement of light chains (Rayment and Winkelmann, 1984). In the maps presented here most of the mass of S1 is contained in the 95-Å-long domain bound to actin (Fig. 4). The junction between this domain and the second domain of S1 at high radius is characterized by an abrupt density change. Correlating the maps with other structural studies (Flicker et al., 1983; Vibert and Craig, 1982; Winkelmann et al., 1984), we conclude that the low density portion of S1 lying at high radius is comprised of parts of the light chains in addition to the portion of the heavy chain linking the head and tail of myosin.

The gross features of the native S1 molecule which we describe are in good agreement with details in projection maps

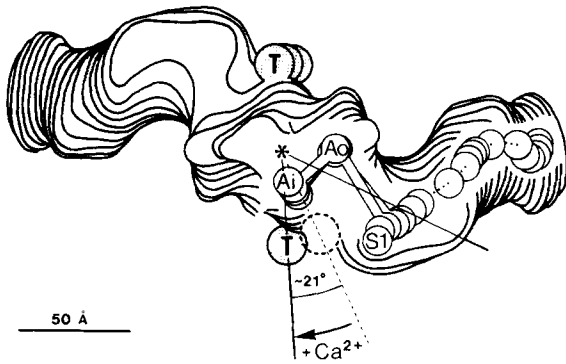


**Figure 8.** Summary of findings showing the structural relationships of actin (Ai and Ao), the myosin head (S1), and tropomyosin (T) in decorated filaments (+Ca<sup>2+</sup>). The azimuthal angle between tropomyosin and the approximate center of mass of actin is 62° (angle between the solid radial lines). The dotted circle shows the estimated location of tropomyosin in the absence of Ca<sup>2+</sup> (based on the work of Haselgrove, 1972; Huxley, 1972; and Parry and Squire, 1973). This location is related to that in activated filaments by a 15 Å (~21°) azimuthal shift. In this model for the regulated filament, tropomyosin remains in contact with the inner domain of actin and does not eclipse the major site of actin–myosin interaction (between Ao and S1).

calculated from thin sections of plastic-embedded 3-D S1 crystals (Winkelmann et al., 1985). However, the maps differ in the apparent length of S1. Winkelmann et al. (1985) conclude that this S1 is at least 160-Å long. Rotary shadowing of similar S1 molecules has given length estimates of ~190 Å (Elliot and Offer, 1978; Flicker et al., 1983, see also Craig et al., 1986). In our maps the longest chord of S1 measures 125–130 Å. Furthermore, the figure is less than this after the layer-line data have been adjusted to compensate for the effects of the CTF (see Materials and Methods). These observations, coupled with density differences along the length of S1, are consistent with the idea that the two domains of S1 are ordered to differing degrees. In the maps the 95-Å-long actin-binding domain is of high density; this suggests that it conforms closely to the helical symmetry of the filament and is firmly attached to actin. In contrast, the abrupt density change at the junction of the two S1 domains and the appearance of the low density domain suggest that this high radius feature does not conform well to the symmetry of the helix. Variability in position of the S1 tail would, after averaging, result in an apparently short S1 and may account for the azimuthal spread of density in this region of the maps.

### **Interaction of Actin, S1, and Tropomyosin**

In one model of the decorated filament (see Amos, 1985, for review), a single S1 spans the long pitch groove formed by the two strands of actin and makes contact with two actin monomers. Tropomyosin is bound to actin behind the S1 binding site and lies within the curve of the S1 molecule. Our results concerning the geometry of binding and the position of tropomyosin relative to the actin–myosin binding site are in conflict with this model and are more in agreement with the model proposed originally by Huxley (1972) and with the recent results of Toyoshima and Wakabayashi (1985b). We find that S1 approaches the actin filament in a tangential fash-

ion and binds to a single actin molecule. Although the binding site appears to cover an entire long face of the actin monomer, the major connectivity and presumably the most intimate contact is between S1 and the outer domain of actin. These details of the native density distribution are seen consistently in the three average maps (two from decorated thin filaments, one from decorated actin), which we have calculated in the course of our work.

We have also demonstrated that in the decorated thin filament (+Ca<sup>2+</sup>) extra density lies in front of the actin–myosin binding site at a radius of ~40 Å (Fig. 7). The most likely interpretation of this finding is that it identifies the position of tropomyosin. Assuming a molecular length of 410 Å for tropomyosin (Phillips et al., 1979), this radial position dictates an axial repeat of 390 Å for the molecule in the thin filament. This figure is in good agreement with measurements of the spacing between troponin complexes in filaments (Ohtsuki, 1975; Spudich et al., 1972). In the maps, tropomyosin is bound to the inner domain of actin, a position similar to that found by O'Brien et al. (1983). Here it is in close proximity to the tip of the S1 molecule rather than within the curve of the S1, as was suggested by others (e.g., Amos et al., 1982).

### **Regulation of Muscular Contraction**

It is of interest to re-examine current views of thin filament-based regulation in the light of our results on the native structure of decorated filaments. The steric blocking theory (Huxley, 1972; Spudich et al., 1972) states that tropomyosin can occupy two different sites in the thin filament. In the absence of Ca<sup>2+</sup>, tropomyosin lies on the S1-binding site and prevents the attachment of S1 to actin. With Ca<sup>2+</sup> present, tropomyosin occupies a second position away from the binding site and thus allows S1 to bind. There is ample evidence for the movement of tropomyosin during thin filament activation (Haselgrove, 1972; Huxley, 1972; Parry and Squire, 1973; Wakabayashi et al., 1975). However, the molecular mechanism by which contraction is regulated remains in doubt. In support of simple steric blocking are results from time-resolved x-ray diffraction studies on muscle during activation (Kress et al., 1986). This work shows that the movement of tropomyosin precedes crossbridge attachment by 12–17 ms, suggesting that it is a prerequisite for myosin binding. In contrast, experiments *in vitro* show that S1 does bind to thin filaments in the absence of Ca<sup>2+</sup> but appears unable to complete the cycle of interaction (Chalovich and Eisenberg, 1982). Chalovich and Eisenberg have suggested that tropomyosin interferes with a kinetic step in the crossbridge cycle, perhaps the release of phosphate from S1.

Based on the work of Haselgrove (1972), Huxley (1972), and Parry and Squire (1973) we have estimated the position of tropomyosin in the thin filament in the absence of Ca<sup>2+</sup> (Fig. 8). In this position, tropomyosin does not totally eclipse the major site of interaction between S1 and Ao but may obscure the contact between the tip of S1 and Ai. It is apparent that this model is compatible with both views of the mechanism of regulation. Coverage of the binding site by tropomyosin may be sufficient to abolish crossbridge attachment. Alternatively, as such a large fraction of the site apparently remains accessible, it is conceivable that S1 can bind to actin, perhaps forming a weakly bound state as envisioned

by Greene and Eisenberg (1980). Clearly, direct determination of the position of tropomyosin in the absence of  $\text{Ca}^{2+}$  will be an important key to understanding the molecular basis of thin filament-based regulation.

We thank Jim Spudich, Nigel Unwin, and Peter Vibert for their help and Don Winkelmann for providing us with abundant quantities of S1. Ken Taylor provided one of the programs used in the statistical analyses. We also thank Anne MacIntyre for preparing the manuscript.

This work was supported by grants GM-25240 and GM-30387 from the National Institutes of Health (to J. A. Spudich) and GM-27764 (to P. N. T. Unwin), and a postdoctoral fellowship from The Muscular Dystrophy Association (to P. F. Flicker).

Received for publication 2 October 1986, and in revised form 23 March 1987.

## References

- Amos, L. A. 1985. Structure of muscle filaments studied by electron microscopy. *Annu. Rev. Biophys. Biophys. Chem.* 14:291-313.
- Amos, L. A., H. E. Huxley, K. C. Holmes, R. S. Goody, and K. A. Taylor. 1982. Structural evidence that myosin heads may interact with two sites on F-actin. *Nature (Lond.)* 299:467-469.
- Amos, L. A., and A. Klug. 1974. Arrangement of subunits in flagellar microtubules. *J. Cell Sci.* 14:523-549.
- Brisson, A., and P. N. T. Unwin. 1985. Quaternary structure of the acetylcholine receptor. *Nature (Lond.)* 1985: 315:474-477.
- Chalovich, J. M., and E. Eisenberg. 1982. Inhibition of actomyosin ATPase activity by troponin-tropomyosin without blocking the binding of myosin to actin. *J. Biol. Chem.* 257:2432-2437.
- Craig, R., J. Trinick, and P. Knight. 1986. Discrepancies in length of myosin head. *Nature (Lond.)* 1986: 320:688.
- DeRosier, D. J., and P. B. Moore. 1970. Reconstruction of three-dimensional images from electron micrographs of structures with helical symmetry. *J. Mol. Biol.* 52:355-369.
- Egelman, E. H. 1985. The structure of F-actin. *J. Muscle Res. Cell Motil.* 6:129-151.
- Elliot, A., and G. Offer. 1978. Shape and flexibility of the myosin molecule. *J. Mol. Biol.* 123:505-519.
- Erickson, H. P., and A. Klug. 1971. Measurement and compensation of defocusing and aberrations by Fourier processing of electron micrographs. *Phil. Trans. R. Soc. Ser. B.* 261:105-118.
- Flicker, P. F., T. Wallimann, and P. Vibert. 1983. Electron microscopy of scallop myosin: location of regulatory light chains. *J. Mol. Biol.* 169:723-741.
- Goody, R. S., M. C. Reedy, W. Hofmann, K. C. Holmes, and M. K. Reedy. 1985. Binding of myosin subfragment 1 to glycerinated insect flight muscle in the rigor state. *Biophys. J.* 47:151-169.
- Greene, L. E., and E. Eisenberg. 1980. Cooperative binding of myosin subfragment-1 to the actin-troponin-tropomyosin complex. *Proc. Natl. Acad. Sci. USA.* 77:2616-2620.
- Haselgrove, J. C. 1972. X-ray evidence for a conformational change in the actin-containing filaments of vertebrate striated muscle. *Cold Spring Harbor Symp. Quant. Biol.* 37:341-352.
- Homo, J.-C., F. Booy, P. Labouesse, J. Lepault, and J. Dubochet. 1984. Improved anticontaminator for cryo-electron microscopy with a Philips EM 400. *J. Microsc.* 136:337-340.
- Huxley, H. E. 1972. Structural changes in the actin- and myosin-containing filaments during contraction. *Cold Spring Harbor Symp. Quant. Biol.* 37:361-376.
- Kabsch, W., H. G. Mannherz, and D. Suck. 1985. Three-dimensional structure of the complex of actin and DNase I at 4.5 Å resolution. *EMBO (Eur. Mol. Biol. Organ.) J.* 4:2113-2118.
- Kendrick-Jones, J., W. Lehman, and A. G. Szent-Györgyi. 1970. Regulation in molluscan muscles. *J. Cell Biol.* 54:313-326.
- Kress, M., H. E. Huxley, A. R. Faruqi, and J. Hendrix. 1986. Structural changes during activation of frog muscle studied by time-resolved X-ray diffraction. *J. Mol. Biol.* 188:325-342.
- Lepault, J., F. P. Booy, and J. Dubochet. 1983. Electron microscopy of frozen biological suspensions. *J. Microsc.* 129:89-102.
- Milligan, R. A. 1985. The native structure of the ribosome: electron crystallography of 2-D crystals in frozen solution. Ph.D. thesis. Stanford University.
- Milligan, R. A., A. Brisson, and P. N. T. Unwin. 1984. Molecular structure determination of crystalline specimens in frozen aqueous solution. *Ultramicroscopy.* 13:1-10.
- Moore, P. B., H. E. Huxley, and D. J. DeRosier. 1970. Three-dimensional reconstruction of F-actin, thin filaments and decorated thin filaments. *J. Mol. Biol.* 50:279-295.
- O'Brien, E. J., J. Couch, G. R. P. Johnson, and E. P. Morris. 1983. Structure of actin and the thin filament. In *Actin: Structure and Function in Muscle and Non-Muscle Cells*. C. G. dos Remedios and J. A. Barden, editors. Academic Press, Australia. 3-16.
- Ohtsuki, I. 1975. Distribution of troponin components in the thin filament studied by immunoelectron microscopy. *J. Biochem.* 77:633-639.
- Pardee, J. D., and J. A. Spudich. 1982. Purification of muscle actin. *Methods Enzymol.* 85:164-181.
- Parry, D. A. D., and J. M. Squire. 1973. Structural role of tropomyosin in muscle regulation: analysis of the x-ray diffraction patterns from relaxed and contracting muscles. *J. Mol. Biol.* 75:33-55.
- Phillips, G. N. Jr., E. E. Lattman, P. Cummins, K. Y. Lee, and C. Cohen. 1979. Crystal structure and molecular interactions of tropomyosin. *Nature (Lond.)* 278:413-417.
- Rayment, I., and D. A. Winkelmann. 1984. Crystallization of myosin subfragment 1. *Proc. Natl. Acad. Sci. USA.* 81:4378-4380.
- Sakabe, N., K. Sakabe, K. Sasaki, H. Kondo, T. Ema, N. Kamiya, and M. Matsushima. 1983. Crystallographic studies of the chicken gizzard G-actin. DNase 1 complex at 5 Å resolution. *J. Biochem.* 93:299-302.
- Schutt, C. E., N. Strauss, K. Morikawa, H. Road, and U. Lindberg. 1985. Crystallographic studies on the profilin:actin complex. In *Actin: Structure and Functions*. T. Yanagida, editor. 11th Taniguchi International Symposium, Taniguchi Foundation, Japan. 10-17.
- Spudich, J. A., and S. Watt. 1971. The regulation of rabbit skeletal muscle contraction. I. Biochemical studies of the interaction of the tropomyosin-troponin complex with actin and the proteolytic fragments of myosin. *J. Biol. Chem.* 246:4866-4871.
- Spudich, J. A., H. E. Huxley, and J. T. Finch. 1972. Regulation of skeletal muscle contraction II. Structural studies of the interaction of tropomyosin-troponin complex with actin. *J. Mol. Biol.* 72:619-632.
- Suck, D., W. Kabsch, and H. G. Mannherz. 1981. Three-dimensional structure of the complex of skeletal muscle actin and bovine pancreatic DNase I at 6 Å resolution. *Proc. Natl. Acad. Sci. USA.* 78:4319-4323.
- Taylor, K. A., and L. A. Amos. 1981. A new model for the geometry of the binding of myosin crossbridges to muscle thin filaments. *J. Mol. Biol.* 147:297-324.
- Toyoshima, C., and T. Wakabayashi. 1985a. Three-dimensional image analysis of the complex of thin filaments and myosin molecules from skeletal muscle. IV. Reconstruction from minimal- and high-dose images of the actin-tropomyosin-myosin subfragment-1 complex. *J. Biochem.* 97:219-243.
- Toyoshima, C., and T. Wakabayashi. 1985b. Three-dimensional image analysis of the complex of thin filaments and myosin molecules from skeletal muscle. V. Assignment of actin in the actin-tropomyosin-myosin subfragment-1 complex. *J. Biochem.* 97:245-263.
- Trinick, J., J. Cooper, J. Seymour, and E. H. Egelman. 1986. Cryo-electron microscopy and three-dimensional reconstruction of actin filaments. *J. Microsc.* 141:349-360.
- Trus, B. L., and A. C. Steven. 1984. Diffraction patterns from stained and unstained helices: consistence or contradiction? *Ultramicroscopy.* 15:325-336.
- Unwin, P. N. T., and P. D. Ennis. 1984. Two configurations of a channel-forming membrane protein. *Nature (Lond.)* 307:609-613.
- Vibert, P., and R. Craig. 1982. Three-dimensional reconstruction of thin filaments decorated with  $\text{Ca}^{2+}$ -regulated myosin. *J. Mol. Biol.* 157:299-319.
- Vibert, P. J., J. C. Haselgrove, J. Lowy, and F. R. Poulsen. 1972. Structural changes in actin-containing filaments of muscle. *J. Mol. Biol.* 71:757-767.
- Wakabayashi, T., H. E. Huxley, L. A. Amos, and A. Klug. 1975. Three-dimensional reconstruction of actin-tropomyosin complex and actin-tropomyosin-troponin T-troponin I complex. *J. Mol. Biol.* 93:477-497.
- Winkelmann, D. A., S. Almeda, P. Vibert, and C. Cohen. 1984. A new myosin fragment: visualization of the regulatory domain. *Nature (Lond.)* 307:758-760.
- Winkelmann, D. A., S. Lowey, and J. L. Press. 1983. Monoclonal antibodies localize changes in myosin heavy chain isoenzymes during avian myogenesis. *Cell.* 34:295-306.
- Winkelmann, D. A., H. Mekeel, and I. Rayment. 1985. Packing analysis of crystalline myosin subfragment-1, Implications for the size and shape of the myosin head. *J. Mol. Biol.* 181:487-501.